Monthly Notices of the ROYAL ASTRONOMICAL SOCIETY

MNRAS **517,** 4070–4080 (2022) https://doi.org/10.1093/mnras/stac2623
Advance Access publication 2022 September 17

FASTCHEM 2 : an improved computer program to determine the gas-phase chemical equilibrium composition for arbitrary element distributions

Joachim W. Stock,⋆ Daniel Kitzmann [1]⋆ and A. Beate C. Patzer[2]

[1]*Center for Space and Habitability, University of Bern, Gesellschaftsstrasse 6, CH-3012 Bern, Switzerland*
[2]*Zentrum für Astronomie und Astrophysik (ZAA), Technische Universität Berlin (TUB), Hardenbergstr. 36, D-10623 Berlin, Germany*

Downloaded from https://academic.oup.com/mnras/article/517/3/4070/6702739 by Universitaetsbibliothek Bern user on 08 March 2023

Accepted 2022 September 12. Received 2022 September 12; in original form 2022 June 16

ABSTRACT

The computation of complex neutral/ionized chemical equilibrium compositions is invaluable to obtain scientific insights of, for example, the atmospheres of extrasolar planets and cool stars. We present FASTCHEM 2 , a new version of the established semi-analytical thermochemical equilibrium code FASTCHEM. Whereas the original version is limited to atmospheres containing a significant amount of hydrogen, FASTCHEM 2 is also applicable to chemical mixtures dominated by any other species, such as CO_2 or N_2. The new C++ code and an optional PYTHON module are publicly available under the GPLv3 license. The program is backward compatible so that the previous version can be easily substituted. We updated the thermochemical data base by adding HNC, FeH, TiH, Ca^-, and some organic molecules. In total 523 species are now in the thermochemical data base including 28 chemical elements. The user can reduce the total number of species to, for example, increase the computation performance or can add further species if the thermochemical data are available. The program is validated against its previous version and extensively tested over an extended pressure–temperature grid with pressures ranging from 10^{-13} up to 10^3 bar and temperatures between 100 and 6000 K. FASTCHEM 2 is successfully applied to a number of different scenarios including nitrogen-, carbon-, and oxygen-dominated atmospheres and test cases without hydrogen and helium. Averaged over the extended pressure–temperature grid FASTCHEM 2 is up to 50 times faster than the previous version and is also applicable to situations not treatable with version 1.

Key words: astrochemistry – methods: numerical – planets and satellites: atmospheres – stars: atmospheres.

1 INTRODUCTION

To gain a detailed scientific understanding of astrophysical objects, such as e.g. the atmospheres of extrasolar planets, protoplanetary discs, or cool stars, the computation of their often complex chemical compositions is indispensable. Therefore, rapid and efficient computer programs are needed. The chemical equilibrium (CE) situation is thermodynamically determined by the minimum of the Gibbs free energy of the system (see e.g. Denbigh 1955; Aris 1969). In combination with the conservation of elements the resulting CE composition can be numerically calculated by minimizing the Gibbs free energy directly (e.g. White, Johnson & Dantzig 1957, 1958) or by employing the law of mass action[1] (e.g. Brinkley 1947). Detailed descriptions of various numerical methods to compute CE compositions can be found in the textbooks by van Zeggeren & Storey (1970) or Smith & Missen (1982), for example.

Assuming CE, Russell (1934) was able to estimate the chemical composition of stellar atmospheres with a then laborious procedure restricted to diatomic molecules and a strictly hierarchical structure of the chemical element abundances. Russell's method became more feasible with the use of electronic computers and has been further developed to account for larger molecules and more species by utilizing the Newton–Raphson method. Such methods have been applied to investigate, for example, cool stellar atmospheres (Vardya 1966; Tsuji 1973; Johnson & Sauval 1982), circumstellar dust shells of asymptotic giant branch (AGB) stars (Gail, Keller & Sedlmayr 1984; Gail & Sedlmayr 1986, 1987; Dominik et al. 1990; Winters, Dominik & Sedlmayr 1994; Ferrarotti & Gail 2001), brown dwarfs (Burrows et al. 2002; Marley et al. 2002; Helling et al. 2008a,b), and to some extend the atmospheres of extrasolar planets (Madhusudhan, Burrows & Currie 2011; Kataria et al. 2014; Morley et al. 2015). To further explore the chemical composition of planetary atmospheres and atmospheres of brown dwarfs under CE conditions, codes such as CONDOR (Lodders & Fegley 1993), TECA (Venot et al. 2012), TEA (Blecic, Harrington & Bowman 2016), GGCHEM (Woitke et al. 2018), and FASTCHEM (Stock et al. 2018) were developed.

FASTCHEM is so far applied to situations, where the CE approximation appears to be reasonable, i.e. the chemical time-scale is considerably shorter than the dynamical time-scale, and non-CE processes, such as e.g. photochemical processes or cosmic ray induced processes, can be neglected. The applications of FASTCHEM include for example particular atmospheric regions of the extrasolar

⋆ E-mail: joachimstock14@gmail.com (JWS); daniel.kitzmann@unibe.ch (DK)

[1]The empirical law of mass action (Guldberg & Waage 1864, 1867, 1879) can be mathematically derived by minimizing the Gibbs free energy (see e.g. Aris 1969).

© 2022 The Author(s)
Published by Oxford University Press on behalf of Royal Astronomical Society

planets KELT-9b (Hoeijmakers et al. 2018, 2019; Hooton et al. 2018; Kitzmann et al. 2018; Fisher et al. 2020; Pino et al. 2020; Wong et al. 2020), KELT-20b/MASCARA-2b (Hoeijmakers et al. 2020a; Nugroho et al. 2020a; Rainer et al. 2021; Johnson et al. 2022), WASP-19b (Sedaghati et al. 2021), WASP-33b (Nugroho et al. 2020b, 2021), WASP-76b (Seidel et al. 2021; Savel et al. 2022), WASP-121b (Hoeijmakers et al. 2020b), WASP-189b (Prinoth et al. 2022), TOI-1518b (Cabot et al. 2021), TOI-2109b (Wong et al. 2021), HD 149026b (Ishizuka et al. 2021), HD 332231b (Sedaghati et al. 2022), and HAT-P-70b (Bello-Arufe et al. 2022). In particular, FASTCHEM is used to determine the chemical composition that is essential for self-consistent modelling of their respective atmospheres. As a result, these models helped for example to detect or confirm neutral and ionized species such as e.g. Ca, Ca^+, Cr, Cr^+, Fe, Fe^+, H, OH, Mg, Mn, Na, Ni, TiO, Sc^+, Ti, Ti^+, V, and Y^+ in the atmospheres of extrasolar planets. FASTCHEM is also employed for comparison with non-equilibrium conditions, e.g. to study the impact of photochemistry, transport, emissions (Mendonça et al. 2018; Charnay et al. 2022; Itcovitz et al. 2022), and for validation of photochemical models (Tsai et al. 2018; Hobbs et al. 2021). Moreover, FASTCHEM has been combined with the exoplanet atmosphere model HELIOS (Malik et al. 2017, 2019a), the opacity calculator HELIOS-K (Grimm & Heng 2015), and/or the observation simulator HELIOS-O (Bower et al. 2019) in various applications (e.g. Linder et al. 2019; Malik et al. 2019b; Grenfell et al. 2020; Morris et al. 2020; Oreshenko et al. 2020; Tabernero et al. 2020; Fossati et al. 2021; Zilinskas et al. 2021; Deitrick et al. 2022; Feinstein et al. 2022; Guzmán-Mesa et al. 2022; Herman et al. 2022; Marleau et al. 2022; Zieba et al. 2022). Other applications of FASTCHEM are the combination with the spectral characterization tool PETITRADTRANS (Mollière et al. 2019) and as a plug-in for the retrieval code TAUREX 3.1 (Al-Refaie et al. 2021, 2022). The recently developed gas opacity generator OPTAB (Hirose et al. 2022) is also compatible with FASTCHEM. Moreover, FASTCHEM was coupled to the photochemical kinetics code VULCAN (Tsai et al. 2017; Shulyak et al. 2020; Zilinskas et al. 2020; Dash et al. 2022) to provide initial values.

Here, we present a new version of FASTCHEM henceforth called FASTCHEM 2. In contrast to the previous version (FASTCHEM 1), FASTCHEM 2 does not rely on the presence of hydrogen as a reference element. The basic equations are now written in a way that neither a specific reference element nor a conversion between the gas pressure and the total hydrogen nuclei number density are explicitly required for the calculation. Therefore, the new program can be applied to chemical element compositions even in total absence of hydrogen. As another improvement, we now follow a semi-analytical approach for the calculation of the electron number density, if the absolute value of the ionization degree of a species is less or equal 1. However, if the user provides thermochemical data including species with higher ionization degrees, FASTCHEM 2 switches automatically to the method used in the previous version. All these changes lead to a significant increase in computational performance, enabling a wider range of applications with higher speed.

In addition, some new species are added and thermochemical data are updated in this study. These include hydrides, phosphides, sulphides, and some organic molecules with potential relevance to atmospheric chemistry. Finally, we provide an optional PYTHON package PYFASTCHEM that allows FASTCHEM 2 to be called directly from within PYTHON scripts. FASTCHEM 2 is backward compatible and the previous version can be easily replaced.

2 METHOD

In accordance with Stock et al. (2018), we denominate the set of all chemical elements with $\mathcal{E} = \left\{E_1, \ldots, E_{|\mathcal{E}|}\right\}$ and the set of all species in the gas phase with $\mathcal{S} = \left\{S_1, \ldots, S_{|\mathcal{S}|}\right\}$. $\mathcal{S}$ includes for example free atoms, molecules, and ions, whereas $\mathcal{E}$ includes solely chemical elements. $|\mathcal{E}|$ is the total number of chemical elements and $|\mathcal{S}|$ is the total number of species treated. Because $\mathcal{E} \subset \mathcal{S}$, $|\mathcal{S}|$ is larger than $|\mathcal{E}|$. The subset $\mathcal{S}$ without the chemical elements in atomic form is denoted by $\mathcal{S} \setminus \mathcal{E}$. The index 0 refers here to the electron, i.e. $\mathcal{E}_0$ is the set of all chemical elements and $\mathcal{S}_0$ the set of all species both including the electron. To determine the CE composition, dissociative equilibrium is assumed, where the dissociation reaction

$$S_i \leftrightharpoons \nu_{i0} E_0 + \nu_{i1} E_1 + \cdots + \nu_{ij} E_j + \cdots = \sum_{j \in \mathcal{E}_0} \nu_{ij} E_j \tag{1}$$

is considered for each species $S_i \in \mathcal{S} \setminus \mathcal{E}$. If $j \neq 0$, the coefficients ν_{ij} of the stoichiometric matrix are non-negative integer numbers. For cations ν_{i0} is negative and for anions the respective coefficient ν_{i0} is positive. Consider for example the cation X^+, the associated dissociation reaction is

$$X^+ \leftrightharpoons X - e^- \tag{2}$$

and $\nu_{X^+0} = -1$. Likewise for the anion X^-, the dissociation reaction is given by

$$X^- \leftrightharpoons X + e^- \tag{3}$$

and $\nu_{X^-0} = 1$.

The sum of all nuclei of the reference element r per unit volume is by definition

$$n_{\langle r \rangle} := n_r + \sum_{i \in \mathcal{S} \setminus \mathcal{E}} \nu_{ir} n_i, \tag{4}$$

where n_r is the number density of the free atoms of the reference element r. Note that in contrast to Stock et al. (2018), the reference element is not necessarily set to be hydrogen.

The CE composition $\left\{n_0, \ldots, n_{|\mathcal{S}_0|}\right\}$ can be calculated using the law of mass action (Guldberg & Waage 1864, 1867, 1879),[2]

$$n_i = K_i \prod_{j \in \mathcal{E}_0} n_j^{\nu_{ij}}, \qquad \forall i \in \mathcal{S} \setminus \mathcal{E}, \tag{5}$$

where n_i is the number density of species i and K_i the temperature-dependent mass action constant, in combination with the element and charge conservation equations:

$$\epsilon_{r,j} n_{\langle r \rangle} = n_j + \sum_{i \in \mathcal{S} \setminus \mathcal{E}} \nu_{ij} n_i, \qquad \forall j \in \mathcal{E}_0, \tag{6}$$

where $\epsilon_{r,j}$ is the abundance of element $j \in \mathcal{E}_0$ relative to $r \in \mathcal{E}$. Assuming charge neutrality, $\epsilon_{r,0}$ is zero in case of the electron. Additionally, the number densities are constrained by the non-negativity condition

$$n_i \geq 0, \qquad i \in \mathcal{S}_0. \tag{7}$$

So far condensates are not included in FASTCHEM. However, if the set of stable condensates obeying Gibbs' phase rule is known a priori, their impact on the gas phase can be included by adapting the element abundances $\epsilon_{r,j}$ appropriately.

[2]For a standard textbook approach see e.g. Denbigh (1955). Lund (1965) provides a more in-depth historical context.

Downloaded from https://academic.oup.com/mnras/article/517/3/4070/6702739 by Universitaetsbibliothek Bern user on 08 March 2023

2.1 Input and output data

The required input format is essentially the same as for FastChem 1 (Stock et al. 2018) so user created input data files for FastChem 1 can still be used for FastChem 2. Note that we updated the thermochemical data and added some species (see Section 3 for details). The temperature-dependent mass action constants for each molecule or ion S_i are fitted as before,

$$\ln \bar{K}_i(T) = \frac{a_0}{T} + a_1 \ln T + b_0 + b_1 T + b_2 T^2, \qquad \forall i \in \mathcal{S} \setminus \mathcal{E}, \tag{8}$$

with the five fit coefficients a_0, a_1, b_0, b_1, and b_2. The natural logarithm of the dimensionless mass action constants is related to the change in the Gibbs free energy of the dissociation reaction (1) with respect to the standard-state pressure $p^\ominus = 1$ bar $(= 10^5$ Pa) via

$$\ln \bar{K}_i = -\frac{\Delta_r G_i^\ominus(T)}{R\,T}. \tag{9}$$

Although FastChem 2 comes with its own thermochemical data base, additional species can be easily included by the user if their mass action constants are available. Species or even elements can be removed by changing the respective input files, e.g. in order to further increase computational speed for specific purposes.

In contrast to Stock et al. (2018), the relative element abundances $\epsilon_{r,j}$ are automatically normalized to their total sum by FastChem 2 via

$$\hat{\epsilon}_j = \frac{\epsilon_{r,j}}{\sum_{k\in\mathcal{E}} \epsilon_{r,k}} = \frac{10^{x_{r,j}}}{\sum_{k\in\mathcal{E}} 10^{x_{r,k}}}, \qquad j \in \mathcal{E}_0, \tag{10}$$

where the $x_{r,j}$ are provided by the user. In stellar atmospheric theory $x_{r,H}$ is usually set to 12, where r = H is the reference element by choice.[3] Using FastChem 2, this convention does not necessarily need to be taken under consideration while creating an input data file as long as the relative element abundances are consistent. It would not be of advantage to provide $\hat{\epsilon}_j$ directly, since this quantity refers only to a specific element mixture.

The output data file format of the stand-alone C++ version is similar to the one generated by the previous version FastChem 1, which is a formatted file listing the gas pressure p_g, the temperature T, the total gas density n_g, the total number density of all nuclei in the gas phase $n_{\langle g\rangle}$, and the number densities n_i of all species $S_i \in \mathcal{S}_0$. Furthermore, a monitor file is generated that includes information about convergence behaviour. It is highly recommended to check this file after the calculation is completed.

2.2 The FastChem 2 algorithm

In most practical applications the total gas pressure p_g is given instead of $n_{\langle r\rangle}$ or, assuming an ideal gas, the associated pressure $p_{\langle r\rangle} = n_{\langle r\rangle} k_B T$, where k_B denotes the Boltzmann constant. Therefore, p_g needs in general to be converted into $n_{\langle r\rangle}$. For chemical systems such as in H–He-dominated stellar atmospheres, $p_{\langle H\rangle}$ can be reasonably well approximated by relatively simple analytic expressions or numerical schemes (see e.g. Tsuji 1973; Sharp & Huebner 1990; Gail & Sedlmayr 2014). In situations where higher precision is required or the number densities of the leading elements are not well known a priori, an iteration procedure is beneficial (Stock et al. 2018; Woitke et al. 2018).

[3] If hydrogen is the chosen reference element, we use the notation x_j instead of $x_{H,j}$.

Here, we rephrase the governing equations to avoid the iteration in order to increase computational speed via elimination of $n_{\langle r\rangle}$. Furthermore, the new formulation permits to perform all calculations without the explicit use of a reference element r $\in \mathcal{E}$ and hence the p_g–$n_{\langle r\rangle}$ conversion becomes obsolete.

2.2.1 *Preconditioning*

The total gas number density is given by

$$n_g = \sum_{j\in\mathcal{E}_0} n_j + \sum_{i\in\mathcal{S}\setminus\mathcal{E}} n_i. \tag{11}$$

Equations (6), (4), and (11) can be used to eliminate $n_{\langle r\rangle}$ and the number density of the reference element n_r, yielding

$$\sum_{k\in\mathcal{E}_0} a_{jk} n_k = \epsilon_{r,j} n_g - \sum_{i\in\mathcal{S}\setminus\mathcal{E}} \left[\nu_{ij} + \epsilon_{r,j}\left(1-\nu_{ir}\right)\right] n_i, \tag{12}$$

where

$$a_{jk} = \delta_{jk} + \epsilon_{r,j}\left(1-\delta_{rk}\right) \tag{13}$$

and δ_{jk} denotes the Kronecker delta. The left-hand side of equation (12) is linear in the number densities of the elements n_k and can be solved for n_j $(j \in \mathcal{E}_0)$:

$$n_j = \sum_{k\in\mathcal{E}_0} \bar{a}_{jk}\epsilon_{r,k} n_g - \sum_{k\in\mathcal{E}_0}\sum_{i\in\mathcal{S}\setminus\mathcal{E}} \bar{a}_{jk}\left[\nu_{ij} + \epsilon_{r,j}\left(1-\nu_{ir}\right)\right] n_i, \tag{14}$$

where

$$\bar{a}_{jk} = \delta_{jk} - \hat{\epsilon}_j\left(1-\delta_{rk}\right) \tag{15}$$

are the components of the inverse of the matrix (a_{jk}). Substituting $\bar{a}_{jk}$, equation (14) can be further simplified to

$$n_j = \hat{\epsilon}_j n_g - \sum_{i\in\mathcal{S}\setminus\mathcal{E}} \left[\nu_{ij} + \hat{\epsilon}_j \sigma_i\right] n_i, \tag{16}$$

with

$$\sigma_i = 1 - \sum_{j\in\mathcal{E}_0} \nu_{ij}. \tag{17}$$

After utilizing the law of mass action (equation 5), we decompose the equation system (16) into a set of equations each in one variable, namely, n_j $(j \in \mathcal{E})$,

$$\hat{\epsilon}_j n_g = n_j + \sum_{k=1}^{N_j} n_j^k \sum_{\substack{i\in\mathcal{S}\setminus\mathcal{E}\\ \nu_{ij}=k\\ \hat{\epsilon}_i=\hat{\epsilon}_j}} \left[\nu_{ij} + \hat{\epsilon}_j\sigma_i\right] K_i \prod_{\substack{l\in\mathcal{E}_0\\ l\neq j}} n_l^{\nu_{il}} + \bar{n}_j + n_{j,\min}, \tag{18}$$

similar to Stock et al. (2018), where

$$n_{j,\min} = \sum_{\substack{i\in\mathcal{S}\setminus\mathcal{E}\\ \hat{\epsilon}_i<\hat{\epsilon}_j}} \left[\nu_{ij} + \hat{\epsilon}_j\sigma_i\right] n_i \tag{19}$$

accounts for the contribution of species that consist of elements of which at least one is less abundant than element j. Moreover,

$$\bar{n}_j = \sum_{\substack{i\in\mathcal{S}\setminus\mathcal{E}\\ \hat{\epsilon}_i=\hat{\epsilon}_j}} \hat{\epsilon}_j \sigma_i n_i \tag{20}$$

describes the contribution of species containing elements more abundant than element j. Furthermore, we defined

$$\hat{\epsilon}_i = \min_{j\in\mathcal{E}} \left\{ \hat{\epsilon}_j \,\middle|\, \nu_{ij} \neq 0 \right\}, \qquad i \in \mathcal{S}\setminus\mathcal{E} \tag{21}$$

Downloaded from https://academic.oup.com/mnras/article/517/3/4070/6702739 by Universitaetsbibliothek Bern user on 08 March 2023

and

$$N_j = \max_{i\in\mathcal{S}\setminus\mathcal{E}} \left\{ \nu_{ij} \,\middle|\, \hat{\epsilon}_i = \hat{\epsilon}_j \right\}, \qquad j \in \mathcal{E}. \tag{22}$$

Introducing the following coefficients:

$$A_{j0} = \bar{n}_j + n_{j,\mathrm{min}} - \hat{\epsilon}_j n_{\mathrm{g}}, \tag{23}$$

$$A_{j1} = 1 + \sum_{\substack{i\in\mathcal{S}\setminus\mathcal{E}\\ \nu_{ij}=k\\ \hat{\epsilon}_i=\hat{\epsilon}_j}} \left[1 + \hat{\epsilon}_j\sigma_i\right] K_i \prod_{\substack{l\in\mathcal{E}_0\\ l\neq j}} n_l^{\nu_{il}}, \tag{24}$$

and

$$A_{jk} = \sum_{\substack{i\in\mathcal{S}\setminus\mathcal{E}\\ \nu_{ij}=k\\ \hat{\epsilon}_i=\hat{\epsilon}_j}} \left[k + \hat{\epsilon}_j\sigma_i\right] K_i \prod_{\substack{l\in\mathcal{E}_0\\ l\neq j}} n_l^{\nu_{il}}, \qquad k \geq 2, \tag{25}$$

equation (18) reduces to a polynomial equation

$$P_j(n_j) := \sum_{k=0}^{N_j} A_{jk} n_j^k = 0, \tag{26}$$

which is solved analytically if its degree N_j is smaller or equal to 2 and via the ordinary Newton–Raphson method (e.g. Deuflhard 2004) in one dimension otherwise.

It might happen that A_{j0} becomes positive in the early stages of the iteration. In that case, we solve the full equation

$$\hat{\epsilon}_j n_{\mathrm{g}} = n_j + \sum_{k=1}^{N_j} n_j^k \sum_{\substack{i\in\mathcal{S}\setminus\mathcal{E}\\ \nu_{ij}=k}} \left[k + \hat{\epsilon}_j\sigma_i\right] K_i \prod_{\substack{l\in\mathcal{E}_0\\ l\neq j}} n_l^{\nu_{il}} \tag{27}$$

for element j. Since A_{jk} can become a negative number, it cannot be easily inferred that the objective functions $P_j(n_j)$ are strictly convex for $n_j \geq 0$. However, it can be shown that for certain conditions $P_j(n_j)$ is equivalent to the strictly convex objective function used in FastChem 1 (see Appendix C). Thus, the convergence of the Newton–Raphson method is guaranteed, if the calculated $n_{\langle\mathrm{g}\rangle}$ is sufficiently close to the solution.

2.2.2 *Determination of the electron density*

The electron density is calculated assuming charge neutrality, i.e. $\epsilon_{\mathrm{r},0} = 0$. We distinguish between two cases. If $|\nu_{i0}| \leq 1$ for all $i \in \mathcal{S}$, it follows from equation (6),

$$0 = n_0 \left(1 + \sum_{\substack{i\in\mathcal{S}\setminus\mathcal{E}\\ \nu_{i0}=1}} K_i \prod_{j\in\mathcal{E}} n_j^{\nu_{ij}}\right) - \frac{1}{n_0} \sum_{\substack{i\in\mathcal{S}\setminus\mathcal{E}\\ \nu_{i0}=-1}} K_i \prod_{j\in\mathcal{E}} n_j^{\nu_{ij}}, \tag{28}$$

which is then solved analytically. Otherwise, the electron density is calculated from the sum of the ion densities,

$$n_0 = -\sum_{i\in\mathcal{S}} \nu_{i0} n_i \tag{29}$$

(see e.g. Gail & Sedlmayr 2014). If cancellation of leading digits causes numerical problems, we first try to solve equation (27) for $j = 0$ by employing the ordinary Newton–Raphson method. Therefore, we set the initial value $n_0^{(0)} = Z/(Z+1)\,n_{\mathrm{g}}$, where $Z = |\min_{i\in\mathcal{S}} \nu_{i0}|$. If the Newton–Raphson method still fails to converge, we utilize the method of Nelder and Mead (Nelder & Mead 1965; Lagrias et al. 1997) as described by Stock et al. (2018). To avoid numerical oscillations the resulting electron density $n_0^{(\mu)}$ is modified according to

$$n_0^{(\mu)} \leftarrow \sqrt{n_0^{(\mu)} n_0^{(\mu-1)}}, \tag{30}$$

where μ is the iteration step.

2.2.3 *Computational procedure*

Since FastChem 2 has been developed on the basis of the previous version FastChem 1 (Stock et al. 2018), the computational procedures are clearly similar despite the rephrasing of the governing equations. Specifically, the element conservation equations, in combination with the law of mass action, are solved one by one in descending order, which is automatically determined beforehand, starting with the most abundant element. An iteration procedure ensures a consistent mathematical solution. Because of the new coupling term $\bar{n}_j$ in equation (18) each step, except for step 1, underwent some changes in comparison to the previous version of FastChem.

Step 1. Initial values for the electron density $n_0^{(0)}$ and for the correction terms $n_{j,\mathrm{min}}^{(0)}$ are set and the logarithmic mass action constants $\ln K_i$ are calculated for a given temperature T.

Step 2. The number densities for all atomic species n_j ($j \in \mathcal{E}$) are calculated via equation (18) (or equation 27 if necessary) in descending order, starting with the most abundant element. n_i and $\bar{n}_j$ are updated at once during this step according to equations (5) and (20).

Step 4. $n_{j,\,\mathrm{min}}$ is updated.

Step 5. The electron density n_0 is calculated (see Section 2.2.2).

2.3 Implementation details

Like FastChem 1, the core of version FastChem 2 is also written in C++. Major updates have been made to increase computational performance. FastChem 2 can easily be incorporated into any other astrophysical or atmospherical models by using the provided object class. For example, this is done in the retrieval code HELIOS-R2 (Kitzmann et al. 2020) that can directly use FastChem 2 during its forward model calculations. In addition to the actual FastChem code, the repository contains a C++ stand-alone version that can be used for plain CE calculations and also showcases how FastChem 2 can be coupled to other codes.

As a major addition, we now provide a complete PYTHON interface (PYFASTCHEM) that allows the user to call FastChem directly from within a PYTHON script. The PYFASTCHEM package is also available on the PYTHON Package Index (PyPI) that allows for a straightforward and easy installation of the PYTHON module using the command: `pip install pyfastchem`. Besides the module itself, we also provide a series of scripts that show how FastChem is used within PYTHON, also giving examples on how to, amongst others, change element abundances on the fly. The scripts can be easily adapted by the user for their special computational requirements. By default the PYTHON scripts produce the same general chemistry and monitor output files as the stand-alone C++ version. Furthermore, the PYTHON version has also additional output capabilities, such as saving data of a specific subset of species or directly visualize the FastChem output.

The code is released under a GNU General Public License version 3.0 (GPLv3) licence (Free Software Foundation 2007) and is freely

Downloaded from https://academic.oup.com/mnras/article/517/3/4070/6702739 by Universitaetsbibliothek Bern user on 08 March 2023

Table 1. Updated thermochemical data since the release of FASTCHEM 1 (Stock et al. 2018). Newly added species are marked with an asterisk (∗).

New	Molecule	Reference
∗	CH_4O_2	Dorofeeva, Novikov & Neumann (2001)
∗	$C_2H_2O_2$	Dorofeeva et al. (2001)
∗	$C_2H_2O_4$	Dorofeeva et al. (2001)
∗	$C_2H_3ClO_2$	Dorofeeva et al. (2001)
∗	$C_2H_4O_3$	Dorofeeva et al. (2001)
∗	$C_2H_6O_2$	Dorofeeva et al. (2001)
∗	C_2NO	Dorofeeva et al. (2001)
∗	C_3N_2O	Dorofeeva et al. (2001)
∗	$C_4H_6O_4$	Dorofeeva et al. (2001)
∗	HNC	Goos, Burcat & Ruscic (2022)
∗	Ca^-	Hoeijmakers et al. (2019)
	CaH	Barklem & Collet (2016)
	ClH	Shenyavskaya & Yungman (2004)
	CrH	Barklem & Collet (2016)
	CuH	Barklem & Collet (2016)
	HF	Shenyavskaya & Yungman (2004)
∗	FeH	Barklem & Collet (2016)
	MgH	Barklem & Collet (2016)
	MnH	Barklem & Collet (2016)
	NaH	Barklem & Collet (2016)
	NiH	Barklem & Collet (2016)
	HP	Lodders (1999)
	HS	Lodders (2004)
∗	TiH	Burrows et al. (2005)
	HN	Goos et al. (2022)
	HNO_3	Dorofeeva et al. (2003)
	H_2O_2	Dorofeeva et al. (2003)
	H_2SO_4	Dorofeeva et al. (2003)
	PH_3	Lodders (1999)
	PN	Lodders (1999)
	NS	Lodders (2004)
	SO_2	Lodders (2004)
	PS	Lodders (2004)

available on GitHub repository: https://github.com/exoclime/FastChem. The repository also includes a full user manual in pdf format that provides detailed information and instructions on how to compile the program and run the model. It also lists all available functions that allow the user to interact with FASTCHEM and describes all required and optional input files.

3 ADDITIONAL AND UPDATED THERMOCHEMICAL DATA

The thermochemical data base that comes with FASTCHEM has been refurbished. In particular, we included the data of additional species especially of potential importance for stellar and planetary atmospheres from the literature and also updated the fit coefficients for the calculation of the mass action constants if newer and/or more precise data were at hand. Table 1 provides an overview of the changes in comparison to the previous version of the FASTCHEM data base (see also Stock et al. 2018, their table 2). The associated input file is backward compatible so it can also be applied by users of FASTCHEM 1.

3.1 Hydrides

Since hydrogen is the most abundant chemical element in our Universe, hydrides are expected to be a very important class of molecules in astrophysics. Barklem & Collet (2016) calculated partition functions and equilibrium constants for diatomic molecules based on improved data, specifically dissociation energies D° were taken from Huber & Herzberg (1979), Curtiss et al. (1991), and in particular Luo (2007). For CaH, CrH, CuH, MgH, MnH, NaH, and NiH we fitted Barklem & Collet (2016)'s logarithmic mass action constants after conversion[4] according to equation (8). Furthermore we added FeH and TiH based on data from Barklem & Collet (2016) and Burrows et al. (2005), respectively, and the hydrogen halides HCl and HF based on data published by Shenyavskaya & Yungman (2004). Finally, NH has been updated according to the data provided by Goos et al. (2022).

3.2 Phosphides and sulphides

Lodders (1999, 2004) critically re-evaluated the molecular data of the phosphides HP, PH_3, and NP and the sulphides HS, NS, SO_2, and PS to overcome inconsistencies in the NIST-JANAF Thermochemical Tables (Chase 1998).[5]

3.3 Organic molecules

Dorofeeva et al. (2001) provided molecular data for the organic species bromoacetic acid (CH_2Br–COOH), chloroacetic acid (CH_2Cl–COOH), oxopropanedinitrile (NC–CO–CN), glycolic acid (HO–CH_2–COOH), glyoxal (O=CH–CH = O), cyanooxomethyl ($\dot{O}$CCN), oxalic acid (HO–CO–CO–OH), methyl hydroperoxide (CH_3–O–O–H), dimethyl peroxide (CH_3–O–O–CH_3), and diacetyl peroxide (CH_3–CO–O–O–CO–CH_3) not included so far. These molecules can play a significant role in Earth's tropospheric (non-equilibrium) chemistry. For example, methyl hydroperoxide is a possible end product of the methane oxidation process in the absence of NO and NO_2 (see e.g. Levy 1971; McConnell & McElroy 1971; Warneck, Klippel & Moortgat 1978; Thompson 1980; Logan et al. 1981; Warneck 1988; Wayne 2000). Glyoxal is an observed ring fragmentation product of the reaction between toluene and hydroxyl (Le Bras & LACTOZ Steering Group 1997; Wayne 2000).

Using the full FASTCHEM 2 data base (28 elements, 523 species) in a gas mixture with solar photospheric element composition, glyoxal is the most abundant molecule of all the newly implemented organic species with the molecular formula $C_xH_yO_z$, where x, y, and z are positive integers. Only formyl (H$\dot{C}$O) and formaldehyde (CH_2O) are in general more abundant.

3.4 Other molecules

The molecular properties of nitric acid ($HONO_2$), sulphuric acid (H_2SO_4), and hydrogen peroxide (H_2O_2) are of particular interest for Earth's atmosphere. Thus, the thermochemical data of these molecules were re-evaluated by Dorofeeva et al. (2003) using newer and improved data (e.g. taking into account the effect of internal rotation). Apart from the Earth, H_2SO_4 was detected in the atmosphere of Venus (Pollack et al. 1974; Surkov et al. 1986; Marcq et al. 2018; Titov et al. 2018; Oschlisniok et al. 2021). The presence of H_2O_2 was confirmed in Mars' atmosphere by Clancy, Sandor & Moriarty-Schieven (2004) and Encrenaz et al. (2004).

[4]Note that Barklem & Collet (2016) define the mass action constants using the Guldberg–Waage law in partial pressures, whereas in this work dimensionless constants $\bar{K}_i(T)$ are defined via the Gibbs free reaction energy (see equation 9).

[5]Note that the data of most of these species so far included in the FASTCHEM data base already originate from other sources (cf. Stock et al. 2018).

Downloaded from https://academic.oup.com/mnras/article/517/3/4070/6702739 by Universitaetsbibliothek Bern user on 08 March 2023

Table 2. Element distribution scenarios for different C, H, N, and O abundance combinations. All other elements are set to solar abundances, except for He and Ne that have been omitted in these calculations. The C:H:N:O:Ar ratios of scenarios I, II, IVa, and IVb roughly resemble the atmospheric C:H:N:O:Ar ratios of Earth, Titan, Mars, and Mars with x_C and x_O swapped.

Scenario	x_C	x_H	x_N	x_O
I	4.98	7.33	8.62	8.09
II	9.25	9.86	11.05	6.54
IIIa	8.43	$-\infty$	7.83	8.69
IIIb	8.69	$-\infty$	7.83	8.43
IVa	8.18	4.97	6.93	8.48
IVb	8.48	4.97	6.93	8.18

3.5 Ions

To investigate the chemical composition of the ultrahot Jupiter KELT-9b, Hoeijmakers et al. (2019) calculated fit coefficients compatible with FASTCHEM for singly and doubly ionized atoms based on partition functions using data from Gurvich et al. (1982), Kurucz & Bell (1995), Lide (2004), and Kramida et al. (2021). Furthermore, they added some anions from which we added Ca^- to the data base for the scenarios discussed in the following section. Since doubly ionized cations are only relevant at extremely high temperatures and low pressures, they are not taken into account here. The fit coefficients of the remaining ions are however listed by Hoeijmakers et al. (2019) and can be easily included if the user is interested in them.

4 RESULTS AND DISCUSSION

4.1 Chemical composition

4.1.1 Planetary atmospheric element composition scenarios

To demonstrate the functionality of FASTCHEM 2 for scenarios not dominated by hydrogen, we choose different C:H:N:O:Ar ratios as shown in Table 2. The element abundance of argon $x_{Ar} = 6.40$ is the same for all scenarios. For the remaining elements solar photospheric abundances (Asplund et al. 2009) have been assumed, except for helium and neon, which have been removed from the present calculations, so that the total gas pressure p_g is not dominated by those noble gases. The temperature has been varied between 500 and 6000 K at constant total gas pressure $p_g = 5 \times 10^{-3}$ mbar.

In this paragraph four scenarios are discussed (I, II, IVa, and IVb), two of them with $x_C < x_O$ (I and IVa), two of them with $x_C > x_O$ (II and IVb), two of them with $x_N > \max\{x_C, x_O\}$ (I and II), and two of them fulfilling $x_N < \min\{x_C, x_O\}$ (IVa and IVb). For the calculation of the CE composition of the four scenarios, 26 elements and 519 species are taken into account. The element distribution of the scenarios roughly corresponds to the element distributions in the atmospheres of the Solar system planets Earth (I) and Mars (IVa), and Saturn's moon Titan (II). Furthermore, a scenario IVb has been added, where the element distribution is the same as in scenario IVa, but with the values of x_C and x_O interchanged.

Fig. 1 shows the most abundant species containing C, H, N, and/or O, as well as the electron abundance. In the two left-hand panels x_C is smaller than x_O. In the upper two panels x_N is larger than max $\{x_C, x_O\}$. Unsurprisingly, the most prevalent species in scenarios I and II are N at higher temperatures ($T \gtrsim 5000$ K) and N_2 at lower temperatures ($T \lesssim 5000$ K). In scenario I, x_O is about three orders of magnitude larger than x_C, hence there is ample of oxygen available, forming numerous oxides such as FeO, SiO, SiO_2, and hydroxides, e.g. $Fe(OH)_2$ and $Mg(OH)_2$. In scenario II, x_C exceeds x_O by about three orders of magnitude. Because of the rich abundance of nitrogen and hydrogen, many hydrocarbons and carbon nitrides are present. In scenarios IVa and IVb, x_C and x_O are in the same order of magnitude and nitrogen is less abundant than carbon and oxygen. In the oxygen-rich case (IVa), carbon is locked in CO or CO_2 at lower temperatures. The remaining oxygen is predominantly bound in SiO. In the carbon-rich case, more carbon is available, which leads to the presence of carbon compounds such as C_3, C_5, and SiC_2. We note, these findings might be affected by including condensation processes or additional molecules. At higher temperature, magnesium and iron are ionized. In comparison to scenarios I, IVa, and IVb, the electron mixing ratio in scenario II is relatively low even at very high temperatures, due the low mixing ratio of magnesium and iron (see Table 2).

4.1.2 Two illustrating element compositions without hydrogen and helium

We tested the code for two scenarios without the chemical elements hydrogen and helium, which by nature cannot be successfully treated with FASTCHEM 1. Therefore, we removed hydrogen and helium from the list of elements in the input file and used solar photospheric element abundances (scenario IIIa). Solar photospheric element abundances are used for scenario IIIb, whereby the numerical values of x_C and x_O are swapped. Because of the removal of hydrogen and helium, only 402 species including the 26 elements remain in these two scenarios. Fig. 2 shows the volume mixing ratios of the most abundant carbon, nitrogen, and oxygen compounds. The upper panel shows the oxygen-rich scenario (IIIa) and the lower panel shows the carbon-rich scenario (IIIb). Since hydrogen and helium have been excluded from these test calculations, carbon and oxygen are the most ample elements. Hence CO, due to its large dissociation energy, has a special role in both scenarios, locking up the less abundant element (carbon or oxygen) over a large temperature range (see Fig. 2). In the oxygen-rich scenario (IIIa) the remaining oxygen can be found in species like O, SiO, and CO_2, in the carbon-rich scenario (IIIb) the excess carbon is mostly bound in C_3, C_4N_2, and SiC_2. Evidently, there are no hydrocarbons or hydroxides present. The electron densities are for both scenarios almost identical, since the element abundances for the main electron donating ions (Mg^+, Fe^+, and Si^+) are the same.

4.1.3 Chemical composition based on the evaporated DMM

As a third example with neither hydrogen nor helium, we calculate the CE gas-phase composition of an evaporated Depleted Mid-ocean ridge basalt Mantle (DMM) using an atmospheric pressure–temperature structure. Therefore, the temperature is held constant at $T = 2000$ K and the total gas pressure p_g is varied between 10^{-1} and 10^{-8} bar. These conditions are comparable to those of a volatile-free atmosphere (see e.g. Schaefer & Fegley 2009 and the related discussion of Miguel et al. 2011). Based on the chemical composition of the DMM's major elements (Workman & Hart 2005), we calculate the relative element abundances shown in Table 3. Note that no hydrogen is present, so this scenario cannot be treated with FASTCHEM 1. The total number of species composed of the 14 elements listed in Table 3 is 80. Fig. 3 shows the mixing ratios of important species. Since the DMM is mostly composed of MgO and SiO, the gas mixture associated with the DMM consists predominantly of Mg, SiO, and at very low pressures of O. Note that

Downloaded from https://academic.oup.com/mnras/article/517/3/4070/6702739 by Universitaetsbibliothek Bern user on 08 March 2023

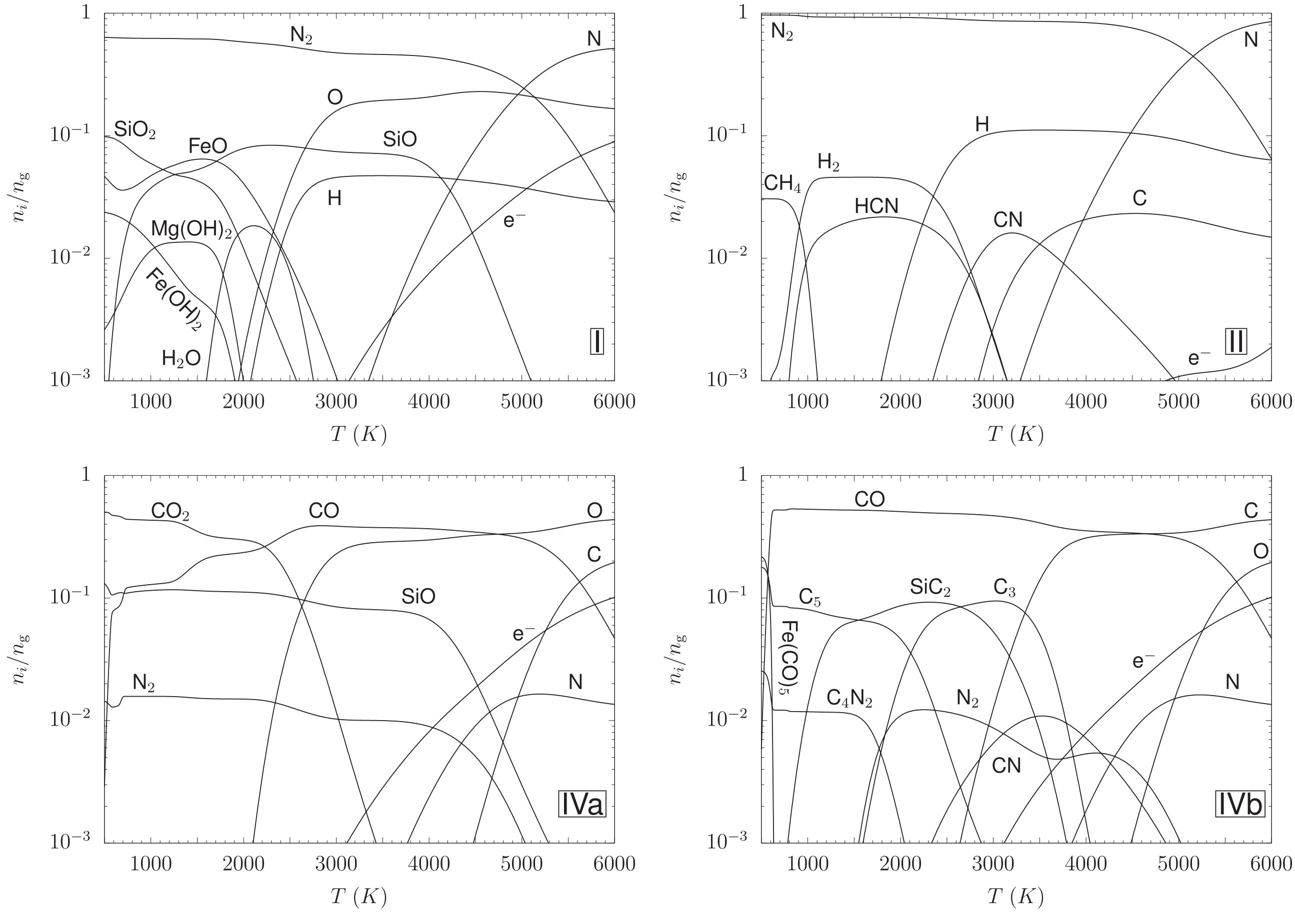

Figure 1. Mixing ratios of the most abundant species, which include the elements C, H, N, and/or O as function of temperature for a fixed total gas pressure $p_g = 5$ mbar and different C:H:N:O:Ar ratios. The element abundances x_C, x_H, x_N, and x_O for the scenarios I, II, IVa, and IVb are given in Table 1.

MgO has a very low dissociation energy in comparison to SiO. Other oxides such as SiO_2, MgO, FeO, CaO, AlO, and O_2 are also present, albeit in less amounts.

4.2 Performance comparison with FastChem 1

The performance differences between FastChem versions 1 and 2 are evaluated in several test calculations with both versions. In particular, we calculate the chemical composition of 62 500 single pressure–temperature combinations on a 250 × 250 pressure–temperature grid considering all 28 elements and 523 species of the FastChem 2 data base. Pressures range from 10^{-13} to 10^3 bar and temperatures from 100 to 6000 K with $\Delta \log T$ and $\Delta \log p_g$ held constant. Additionally, the hydrogen and helium element abundances x_H and x_{He} are varied in these tests. In this section, three distinct cases are discussed.

(i) In the first case only the hydrogen element abundance x_H is varied and the remaining element abundances x_j are fixed at the solar photospheric value.

(ii) In the second scenario the hydrogen and the helium element abundances x_H and x_{He} are varied while keeping the x_H:x_{He} ratio constant.

(iii) The last case is identical to the second but does not include ion chemistry.

The computation time is obtained by taking the arithmetic mean of repeated calculations of the CE composition over the whole p_g–T grid.

Fig. 4 shows the resulting computation time as function of the hydrogen element abundance x_H. The upper panel depicts the average computation time for the complete p_g–T grid relative to the reference scenario (FastChem 2 with ion chemistry for $x_H = 12$). The lower panel shows the ratio between the runtimes of FastChem 1 and FastChem 2. For our test calculations, we use a desktop computer with an Intel i9-7960X processor. The computation time[6] is about 15 s for the whole p_g–T grid.

The results indicate that FastChem 2 is substantially faster than FastChem 1 for all cases (i)–(iii). Even at solar photospheric element abundances, the computation times of version 2 are only 10–20 per cent of the other version. For $x_H > 8$, the computation time of both versions increases with decreasing x_H for all cases. This is mainly due to the decomposition of the system of equations (16) into a set of coupled non-linear equations (18) in one variable each. The resulting competition of other chemical elements such as carbon, nitrogen, and oxygen with hydrogen causes the coefficient A_{j0} to be positive and it becomes necessary to use equation (27) (see Section 2.2.1). This effect reaches its maximum when x_H is of the

[6] Note that the computation time heavily depends on the computer hardware employed.

Downloaded from https://academic.oup.com/mnras/article/517/3/4070/6702739 by Universitaetsbibliothek Bern user on 08 March 2023

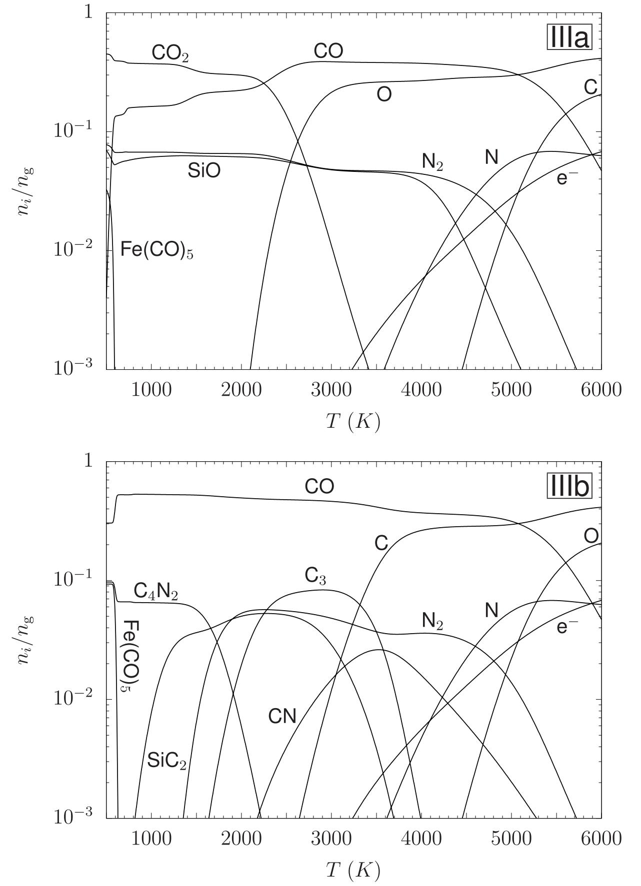

Figure 2. Volume mixing ratios of the most abundant carbons, nitrides, and oxides as function of temperature for a fixed total gas pressure $p_g = 5$ mbar. The element abundances x_C and x_O for the scenarios IIIa and IIIb are given in Table 1.

Table 3. Element abundances relative to oxygen derived from the chemical composition of the DMM estimated by Workman & Hart (2005).

Element		$x_{O,j}$	Element		$x_{O,j}$
O	Oxygen	12.00	Na	Sodium	9.37
Mg	Magnesium	11.73	Ni	Nickel	9.25
Si	Silicon	11.62	Mn	Manganese	9.01
Fe	Iron	10.80	Ti	Titanium	8.96
Ca	Calcium	10.50	P	Phosphorus	8.17
Al	Aluminium	10.34	K	Potassium	7.85
Cr	Chromium	9.62			

same order of magnitude as x_C, x_N, and x_O resulting in a longest computation time at $x_H \approx 8$. For $x_H < 8$, the computation time decreases slightly and then remains relatively constant for decreasing x_H with the chemistry now dominated by oxygen.

If x_H is larger than the solar photospheric helium abundance $x_{He,\,solar}$, the computation time for cases (i) and (ii) is essentially at level. If x_H is smaller than $x_{He,\,solar}$, Fig. 4 (upper panel) indicates qualitative differences. The computation time of FASTCHEM 1 in case (ii) is larger than in case (i). For low hydrogen abundances n_g is determined by n_{He} in version 1. Hence, in contrast to case (ii), the conversion between gas pressure p_g and hydrogen nuclei density $n_{\langle H\rangle}$ is trivial for sufficiently low temperatures (for details see Stock et al. 2018, their section 2.3).

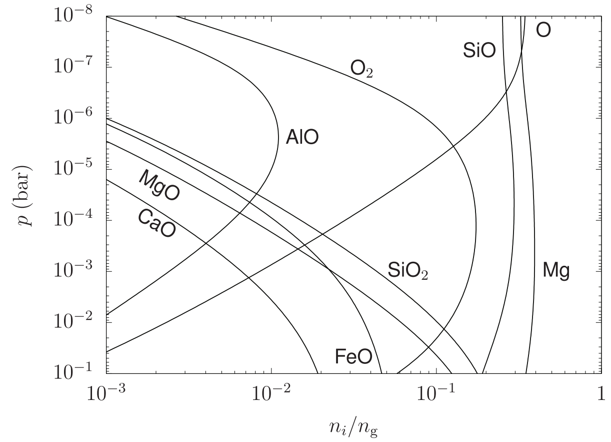

Figure 3. Volume mixing ratios of the most abundant oxides together with atomic magnesium as function of pressure for a constant temperature $T = 2000$ K using the chemical element composition given in Table 3.

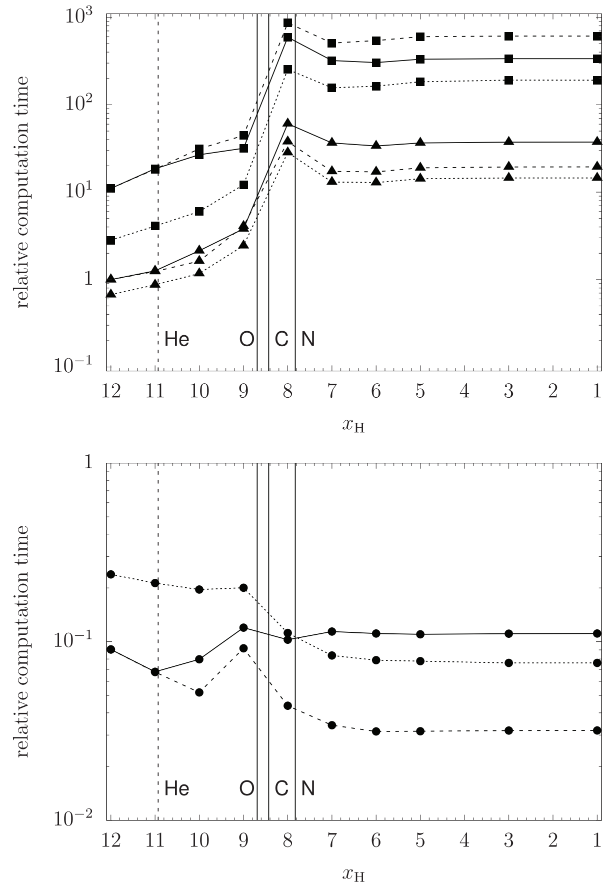

Figure 4. Upper panel: computation time relative to the reference scenario, using FASTCHEM 1 (squares) and FASTCHEM 2 (triangles), averaged over the p_g–T plane (see text). Lower panel: computation time of FASTCHEM 2 relative to FASTCHEM 1. Solid lines refer to case (i), dashed lines to case (ii), and dotted lines to case (iii).

An opposite behaviour can be seen, when applying FASTCHEM 2. Here, the computation time of case (i) is larger than of case (ii). The rationale behind this effect is different from FASTCHEM 1, since here no p_g–$n_{\langle H\rangle}$ conversion is necessary. By inspection of equation (18) it can be recognized that the main difference between case (i) and (ii)

Downloaded from https://academic.oup.com/mnras/article/517/3/4070/6702739 by Universitaetsbibliothek Bern user on 08 March 2023

is the value of $\hat{\epsilon}_j$. For all chemical elements, except of helium, it follows from equation (10), that $\hat{\epsilon}_j$ is in case (ii) larger than in case (i). Hence, the summands in equation (18), which include $\hat{\epsilon}_j$, such as the correction term $n_{j,\,\mathrm{min}}$, have a larger impact on the mathematical solution. Consequently, more iteration steps are needed until convergence is achieved, resulting in an increase in computation time. This is not the case for helium. However, the percentage in computation time of helium in comparison to the remaining elements is relatively modest.

The exclusion of the ion chemistry (case iii) leads to an increased performance between a factor of 3.2 and 5.2 in version 1. In FASTCHEM 2 the performance gain is between 32 per cent and 67 per cent.

With less than 3 per cent of the previous version's runtime at very low hydrogen and helium abundances, FASTCHEM 2 requires only a small fraction of the computational cost, needed by FASTCHEM 1, to perform the same calculations.

5 SUMMARY

We present a new updated version of FASTCHEM, called FASTCHEM 2, for the efficient and computationally fast calculation of chemical gas-phase equilibria. We modified the original FASTCHEM algorithm, so it can handle arbitrary element compositions. Additionally, it can deal now with situations that are not dominated by hydrogen or helium. We added some new species potentially relevant to atmospheric science and updated the thermochemical data used by FASTCHEM 2. The code is validated against FASTCHEM 1 and its functionality is demonstrated on several examples with different element composition over a wide range of pressure and temperature values. A performance comparison shows that FASTCHEM 2 is significantly faster than FASTCHEM 1 up to a factor of 50 in computation time. The program is coded in object oriented C++, but it can be optionally called from within PYTHON scripts using the new PYFASTCHEM package. FASTCHEM 2 and PYFASTCHEM are open source and publicly available at GitHub (https://github.com/exoclime/FastChem) under the GNU General Public License version 3 (GPLv3; Free Software Foundation 2007).

ACKNOWLEDGEMENTS

DK acknowledges financial and administrative support by the Center for Space and Habitability, University of Bern and the PlanetS National Centre of Competence in Research (NCCR).

DATA AVAILABILITY

The data underlying this paper are available in the FASTCHEM GitHub repository, at https://github.com/exoclime/FastChem.

REFERENCES

Al-Refaie A. F., Changeat Q., Waldmann I. P., Tinetti G., 2021, ApJ, 917, 37
Al-Refaie A. F., Changeat Q., Venot O., Waldmann I. P., Tinetti G., 2022, ApJ, 932, 123
Aris R., 1969, Elementary Chemical Reactor Analysis. Prentice-Hall, Englewood Cliffs, NJ
Asplund M., Grevesse N., Sauval A. J., Scott P., 2009, ARA&A, 47, 481
Barklem P. S., Collet R., 2016, A&A, 588, A96
Bello-Arufe A., Cabot S. H. C., Mendonça J. M., Buchhave L. A., Rathcke A. D., 2022, AJ, 163, 96
Blecic J., Harrington J., Bowman M. O., 2016, ApJS, 225, 4
Bower D. J., Kitzmann D., Wolf A. S., Sanan P., Dorn C., Oza A. V., 2019, A&A, 631, A103
Brinkley S. R., Jr, 1947, J. Chem. Phys., 15, 107
Burrows A., Burgasser A. J., Kirkpatrick J. D., Liebert J., Milsom J. A., Sudarsky D., Hubeny I., 2002, ApJ, 573, 394
Burrows A., Dulick M., Bauschlicher C. W. J., Bernath P. F., Ram R. S., Sharp C. M., Milsom J. A., 2005, ApJ, 624, 988
Cabot S. H. C. et al., 2021, AJ, 162, 218
Charnay B. et al., 2022, Exp. Astron., 53, 417
Chase M. W. J., 1998, J. Phys. Chem. Reference Data Monograph, 9, 1
Clancy R. T., Sandor B. J., Moriarty-Schieven G. H., 2004, Icarus, 168, 116
Curtiss L. A., Raghavachari K., Trucks G. W., Pople J. A., 1991, J. Chem. Phys., 94, 7221
Dash S. et al., 2022, ApJ, 932, 20
Deitrick R., Heng K., Schroffenegger U., Kitzmann D., Grimm S. L., Malik M., Mendonça J. M., Morris B. M., 2022, MNRAS, 512, 3759
Denbigh K., 1955, The Principles of Chemical Equilibrium. Cambridge Univ. Press, Cambridge
Deuflhard P., 2004, Newton Methods for Nonlinear Problems: Affine Invariance and Adaptive Algorithms. Springer-Verlag, Berlin
Dominik C., Gail H. P., Sedlmayr E., Winters J. M., 1990, A&A, 240, 365
Dorofeeva O. V., Novikov V. P., Neumann D. B., 2001, J. Phys. Chem. Reference Data, 30, 475
Dorofeeva O. V., Iorish V. S., Novikov V. P., Neumann D. B., 2003, J. Phys. Chem. Reference Data, 32, 879
Encrenaz T. et al., 2004, Icarus, 170, 424
Feinstein A. D. et al., 2022, AJ, 164, 110
Ferrarotti A. S., Gail H. P., 2001, A&A, 371, 133
Fisher C., Hoeijmakers H. J., Kitzmann D., Márquez-Neila P., Grimm S. L., Sznitman R., Heng K., 2020, AJ, 159, 192
Fossati L., Young M. E., Shulyak D., Koskinen T., Huang C., Cubillos P. E., France K., Sreejith A. G., 2021, A&A, 653, A52
Free Software Foundation, 2007, GNU General Public License v3.0. Available at http://www.gnu.org/licenses/gpl.html
Gail H.-P., Sedlmayr E., 1986, A&A, 166, 225
Gail H.-P., Sedlmayr E., 1987, A&A, 171, 197
Gail H.-P., Sedlmayr E., 2014, Physics and Chemistry of Circumstellar Dust Shells. Cambridge Univ. Press, Cambridge
Gail H.-P., Keller R., Sedlmayr E., 1984, A&A, 133, 320
Goos E., Burcat A., Ruscic B., 2022, Extended Third Millenium Ideal Gas Thermochemical Database with Updates from Active Thermochemical Tables. Available at http://garfield.chem.elte.hu/Burcat/burcat.html
Grenfell J. L., Godolt M., Cabrera J., Carone L., Muñoz A. G., Kitzmann D., Smith A. M. S., Rauer H., 2020, Exp. Astron., 50, 1
Grimm S. L., Heng K., 2015, ApJ, 808, 182
Guldberg C. M., Waage P., 1864, Studier over Affiniteten. Forhandlinger i Videnskabs-selskabet i Christiania. Brøgger & Christie, Christiania, p. 35
Guldberg C. M., Waage P., 1867, Études sur Les Affinités Chimiques. Brøgger & Christie, Christiania
Guldberg C. M., Waage P., 1879, J. Praktische Chem., 19, 69
Gurvich L. V., Veits I. V., Medvedev V. A., Khachkuruzov G. A., Yungman V. S., Bergman G. A., 1982, Termodinamicheski Svoistva Individual'nikh Veshchestv (Thermodynamic Properties of Individual Substances). Nauka, Moscow
Guzmán-Mesa A., Kitzmann D., Mordasini C., Heng K., 2022, MNRAS, 513, 4015
Helling C. et al., 2008a, MNRAS, 391, 1854
Helling C., Dehn M., Woitke P., Hauschildt P. H., 2008b, ApJ, 675, L105
Herman M. K., de Mooij E. J. W., Nugroho S. K., Gibson N. P., Jayawardhana R., 2022, AJ, 163, 248
Hirose S., Hauschildt P., Minoshima T., Tomida K., Sano T., 2022, A&A, 659, A87
Hobbs R., Rimmer P. B., Shorttle O., Madhusudhan N., 2021, MNRAS, 506, 3186
Hoeijmakers H. J. et al., 2018, Nature, 560, 453
Hoeijmakers H. J. et al., 2019, A&A, 627, A165
Hoeijmakers H. J. et al., 2020a, A&A, 641, A120
Hoeijmakers H. J. et al., 2020b, A&A, 641, A123

Downloaded from https://academic.oup.com/mnras/article/517/3/4070/6702739 by Universitaetsbibliothek Bern user on 08 March 2023

Hooton M. J., Watson C. A., de Mooij E. J. W., Gibson N. P., Kitzmann D., 2018, ApJ, 869, L25
Huber K.-P., Herzberg G., 1979, Molecular Spectra and Molecular Structure. IV: Constants of Diatomic Molecules. Van Nostrand Reinhold Company, New York
Ishizuka M., Kawahara H., Nugroho S. K., Kawashima Y., Hirano T., Tamura M., 2021, AJ, 161, 153
Itcovitz J. P., Rae A. S. P., Citron R. I., Stewart S. T., Sinclair C. A., Rimmer P. B., Shorttle O., 2022, Planet. Sci. J., 3, 115
Johnson H. R., Sauval A. J., 1982, A&AS, 49, 77
Johnson M. C. et al., 2022, preprint (arXiv:2205.12162)
Kataria T., Showman A. P., Fortney J. J., Marley M. S., Freedman R. S., 2014, ApJ, 785, 92
Kitzmann D. et al., 2018, ApJ, 863, 183
Kitzmann D., Heng K., Oreshenko M., Grimm S. L., Apai D., Bowler B. P., Burgasser A. J., Marley M. S., 2020, ApJ, 890, 174
Kramida A., Ralchenko Y., Reader J., NIST ASD Team, 2021, NIST Atomic Spectra Database (ver. 5.9). National Institute of Standards and Technology, Gaithersburg, MD. Available at: https://physics.nist.gov/asd
Kurucz R. L., Bell B., 1995, Atomic Line List. Smithsonian Astrophysical Observatory, Cambridge, MA(Kurucz CD-ROM)
Lagrias J. C., Reeds J. A., Wright M. H., Wright P. E., 1997, Convergence Properties of the Nelder-Mead Simplex Algorithm in Low Dimensions. Technical Report, Computing Sciences Research Center, Bell Laboratories, Murray Hill, NJ
Le Bras G., LACTOZ Steering Group, 1997, Chemical Processes in Atmospheric Oxidation. Springer-Verlag, Berlin
Levy H., II, 1971, Science, 173, 141
Lide D. R., 2004, CRC Handbook of Chemistry and Physics, 85th edn. CRC Press, Boca Raton, FL
Linder E. F., Mordasini C., Mollière P., Marleau G.-D., Malik M., Quanz S. P., Meyer M. R., 2019, A&A, 623, A85
Lodders K., 1999, J. Phys. Chem. Reference Data, 28, 1705
Lodders K., 2004, J. Phys. Chem. Reference Data, 33, 357
Lodders K., Fegley B., 1993, Earth Planet. Sci. Lett., 117, 125
Logan J. A., Prather M. J., Wofsy S. C., McElroy M. B., 1981, J. Geophys. Res., 86, 7210
Lund E. W., 1965, J. Chem. Education, 42, 548
Luo Y.-R., 2007, Comprehensive Handbook of Chemical Bond Energies. CRC Press, Boca Raton, FL
McConnell J. C., McElroy M. B., 1971, Nature, 233, 187
Madhusudhan N., Burrows A., Currie T., 2011, ApJ, 737, 34
Malik M. et al., 2017, AJ, 153, 56
Malik M., Kitzmann D., Mendonça J. M., Grimm S. L., Marleau G.-D., Linder E. F., Tsai S.-M., Heng K., 2019a, AJ, 157, 170
Malik M., Kempton E. M. R., Koll D. D. B., Mansfield M., Bean J. L., Kite E., 2019b, ApJ, 886, 142
Marcq E., Mills F. P., Parkinson C. D., Vandaele A. C., 2018, Space Sci. Rev., 214, 10
Marleau G. D. et al., 2022, A&A, 657, A38
Marley M. S., Seager S., Saumon D., Lodders K., Ackerman A. S., Freedman R. S., Fan X., 2002, ApJ, 568, 335
Mendonça J. M., Tsai S.-M., Malik M., Grimm S. L., Heng K., 2018, ApJ, 869, 107
Miguel Y., Kaltenegger L., Fegley B., Schaefer L., 2011, ApJ, 742, L19
Mollière P., Wardenier J. P., van Boekel R., Henning T., Molaverdikhani K., Snellen I. A. G., 2019, A&A, 627, A67
Morley C. V., Fortney J. J., Marley M. S., Zahnle K., Line M., Kempton E., Lewis N., Cahoy K., 2015, ApJ, 815, 110
Morris B. M., Hoeijmakers H. J., Kitzmann D., Demory B.-O., 2020, AJ, 160, 5
Nelder J. A., Mead R., 1965, Comput. J., 7, 308
Nugroho S. K., Gibson N. P., de Mooij E. J. W., Watson C. A., Kawahara H., Merritt S., 2020a, MNRAS, 496, 504
Nugroho S. K., Gibson N. P., de Mooij E. J. W., Herman M. K., Watson C. A., Kawahara H., Merritt S. R., 2020b, ApJ, 898, L31
Nugroho S. K. et al., 2021, ApJ, 910, L9
Oreshenko M. et al., 2020, AJ, 159, 6
Oschlisniok J., Häusler B., Pätzold M., Tellmann S., Bird M. K., Peter K., Andert T. P., 2021, Icarus, 362, 114405
Pino L. et al., 2020, ApJ, 894, L27
Pollack J. B. et al., 1974, Icarus, 23, 8
Prinoth B. et al., 2022, Nat. Astron., 6, 449
Rainer M. et al., 2021, A&A, 649, A29
Russell H. N., 1934, ApJ, 79, 317
Savel A. B. et al., 2022, ApJ, 926, 85
Schaefer L., Fegley B., 2009, ApJ, 703, L113
Sedaghati E. et al., 2021, MNRAS, 505, 435
Sedaghati E. et al., 2022, A&A, 659, A44
Seidel J. V. et al., 2021, A&A, 653, A73
Sharp C. M., Huebner W. F., 1990, ApJS, 72, 417
Shenyavskaya E. A., Yungman V. S., 2004, J. Phys. Chem. Reference Data, 33, 923
Shulyak D., Lara L. M., Rengel M., Nèmec N. E., 2020, A&A, 639, A48
Smith W. R., Missen R. W., 1982, Chemical Reaction Equilibrium Analysis: Theory and Algorithms. Wiley, New York
Stock J. W., Kitzmann D., Patzer A. B. C., Sedlmayr E., 2018, MNRAS, 479, 865
Surkov Y. A. et al., 1986, Soviet Astron. Lett., 12, 44
Tabernero H. M. et al., 2020, MNRAS, 498, 4222
Thompson A. M., 1980, Tellus, 32, 376
Titov D. V., Ignatiev N. I., McGouldrick K., Wilquet V., Wilson C. F., 2018, Space Sci. Rev., 214, 126
Tsai S.-M., Lyons J. R., Grosheintz L., Rimmer P. B., Kitzmann D., Heng K., 2017, ApJS, 228, 20
Tsai S.-M., Kitzmann D., Lyons J. R., Mendonça J., Grimm S. L., Heng K., 2018, ApJ, 862, 31
Tsuji T., 1973, A&A, 23, 411
van Zeggeren F., Storey S. H., 1970, The Computation of Chemical Equilibria. Cambridge Univ. Press, Cambridge
Vardya M. S., 1966, MNRAS, 134, 347
Venot O., Hébrard E., Agúndez M., Dobrijevic M., Selsis F., Hersant F., Iro N., Bounaceur R., 2012, A&A, 546, A43
Warneck P., 1988, in Warneck P., ed., Chemistry of the Natural Atmosphere. Academic Press, New York, p. 131
Warneck P., Klippel W., Moortgat G. K., 1978, Ber. Bunsengesellschaft Phys. Chem., 82, 1136
Wayne R. P., 2000, Chemistry of Atmospheres. Cambridge Univ. Press, Cambridge
White W. B., Johnson S. M., Dantzig G. B., 1957, Chemical Equilibrium in Complex Mixtures. Technical Report. RAND Corp., Santa Monica, CA
White W. B., Johnson S. M., Dantzig G. B., 1958, J. Chem. Phys., 28, 751
Winters J. M., Dominik C., Sedlmayr E., 1994, A&A, 288, 255
Woitke P., Helling C., Hunter G. H., Millard J. D., Turner G. E., Worters M., Blecic J., Stock J. W., 2018, A&A, 614, A1
Wong I. et al., 2020, AJ, 160, 88
Wong I. et al., 2021, AJ, 162, 256
Workman R. K., Hart S. R., 2005, Earth Planet. Sci. Lett., 231, 53
Zieba S. et al., 2022, A&A, 664, A79
Zilinskas M., Miguel Y., Mollière P., Tsai S.-M., 2020, MNRAS, 494, 1490
Zilinskas M., Miguel Y., Lyu Y., Bax M., 2021, MNRAS, 500, 2197

APPENDIX A: TREATMENT OF NUMERICAL OVERFLOW

In some cases numerical overflow could occur, mainly because of the logarithmic mass action constant (equation 9). This might happen for instance at very low temperatures T or large values of Gibbs reaction energies $\Delta_r G_i^{\ominus}(T)$. In order to avoid numerical overflow, equation (26) can be optionally multiplied with a scaling factor $e^{-\psi_j}$,

$$e^{-\psi_j} P_j(n_j) = \sum_{k=0}^{N_j} e^{-\psi_j} A_{jk} n_j^k = \sum_{k=0}^{N_j} \hat{A}_{jk} n_j^k = 0, \qquad \text{(A1)}$$

Downloaded from https://academic.oup.com/mnras/article/517/3/4070/6702739 by Universitaetsbibliothek Bern user on 08 March 2023

with

$$\psi_j := \max_{i\in\mathcal{S}\setminus\mathcal{E}} \left(\ln K_i + \sum_{\substack{l\in\mathcal{E}_0 \\ l\neq j}} \nu_{il} \ln n_l \right) - \xi_j \tag{A2}$$

and $\xi_j \geq 0$ a non-negative constant that depends on the computer system and can be optionally specified by the user. The default value is 0. The modified coefficients are

$$\hat{A}_{j0} = \mathrm{e}^{-\psi_j} A_{j0} = \mathrm{e}^{-\psi_j} \left(\bar{n}_j + n_{j,\min} - \hat{\epsilon}_j n_{\mathrm{g}}\right), \tag{A3}$$

$$\begin{aligned}\hat{A}_{j1} &= \mathrm{e}^{-\psi_j} A_{j1} \\ &= \mathrm{e}^{-\psi_j} + \sum_{\substack{i\in\mathcal{S}\setminus\mathcal{E} \\ \nu_{ij}=k \\ \hat{\epsilon}_i=\hat{\epsilon}_j}} \left[1 + \hat{\epsilon}_j \sigma_i\right] \exp\left\{ \ln K_i + \sum_{\substack{l\in\mathcal{E}_0 \\ l\neq j}} \nu_{il} \ln n_l - \psi_j \right\},\end{aligned} \tag{A4}$$

and

$$\begin{aligned}\hat{A}_{jk} &= \mathrm{e}^{-\psi_j} A_{jk} \\ &= \sum_{\substack{i\in\mathcal{S}\setminus\mathcal{E} \\ \nu_{ij}=k \\ \hat{\epsilon}_i=\hat{\epsilon}_j}} \left[k + \hat{\epsilon}_j \sigma_i\right] \exp\left\{ \ln K_i + \sum_{\substack{l\in\mathcal{E}_0 \\ l\neq j}} \nu_{il} \ln n_l - \psi_j \right\}\end{aligned} \tag{A5}$$

for all $k \geq 2$.

APPENDIX B: ALTERNATIVE DERIVATION OF EQUATION (16)

In this appendix, we outline an alternative derivation of equation (16). This derivation is slightly shorter, but probably less intuitive as the one presented in Section 2.2.1. Instead of using a reference element r, equation (16) can also be derived by making use of the total number density of atomic nuclei:

$$n_{\langle \mathrm{g}\rangle} = \sum_{j\in\mathcal{E}} n_j + \sum_{j\in\mathcal{E}} \sum_{i\in\mathcal{S}\setminus\mathcal{E}} \nu_{ij} n_i. \tag{B1}$$

The element conservation can then be expressed via

$$\hat{\epsilon}_j n_{\langle \mathrm{g}\rangle} = n_j + \sum_{i\in\mathcal{S}\setminus\mathcal{E}} \nu_{ij} n_i, \qquad j \in \mathcal{E}. \tag{B2}$$

By eliminating $\sum_{j\in\mathcal{E}} n_j$ and $n_{\langle \mathrm{g}\rangle}$ from equations (11), (B1), and (B2), one easily obtains equation (16) after some rearrangement. Note that $\hat{\epsilon}_j$ is defined by equation (10) as the normalized relative element abundance. In context of equation (B2), $\hat{\epsilon}_j$ can also be understood as the element abundance relative to the total number density of all atomic nuclei.

APPENDIX C: ON THE OBJECTIVE FUNCTIONS UTILIZED IN FASTCHEM 1 AND FASTCHEM 2

Here, we point out the similarities between the objective functions used in FastChem 1 and FastChem 2. Starting from equation (16), let

$$F_j(n_j) := n_j + \sum_{i\in\mathcal{S}\setminus\mathcal{E}} \left[\nu_{ij} + \hat{\epsilon}_j \sigma_i\right] n_i - \hat{\epsilon}_j n_{\mathrm{g}} \tag{C1}$$

be an objective function. The sum in equation (C1) can be split yielding

$$F_j(n_j) = n_j + \sum_{\substack{i\in\mathcal{S}\setminus\mathcal{E} \\ \hat{\epsilon}_i=\hat{\epsilon}_j}} \left[\nu_{ij} + \hat{\epsilon}_j \sigma_i\right] n_i + \sum_{\substack{i\in\mathcal{S}\setminus\mathcal{E} \\ \hat{\epsilon}_i<\hat{\epsilon}_j}} \left[\nu_{ij} + \hat{\epsilon}_j \sigma_i\right] n_i - \hat{\epsilon}_j n_{\mathrm{g}}. \tag{C2}$$

After defining

$$\tilde{n}_{j,\min} = \sum_{\substack{i\in\mathcal{S}\setminus\mathcal{E} \\ \hat{\epsilon}_i<\hat{\epsilon}_j}} \nu_{ij} n_i \tag{C3}$$

and some straightforward algebraic manipulations, one obtains

$$F_j(n_j) = n_j + \sum_{\substack{i\in\mathcal{S}\setminus\mathcal{E} \\ \hat{\epsilon}_i=\hat{\epsilon}_j}} \nu_{ij} n_i + \tilde{n}_{j,\min} - \hat{\epsilon}_j \left(n_{\mathrm{g}} - \sum_{i\in\mathcal{S}\setminus\mathcal{E}} \sigma_i n_i \right). \tag{C4}$$

The correction term $\tilde{n}_{j,\min}$ is the same as used by Stock et al. (2018) (there denominated by $n_{j,\min}$). Eliminating n_{g} with help of equation (11) and by taking equation (B1) into account, it follows

$$F_j = n_j + \sum_{\substack{i\in\mathcal{S}\setminus\mathcal{E} \\ \hat{\epsilon}_i=\hat{\epsilon}_j}} \nu_{ij} n_i + \tilde{n}_{j,\min} - \hat{\epsilon}_j n_{\langle \mathrm{g}\rangle}. \tag{C5}$$

Because

$$n_{\langle \mathrm{g}\rangle} = \sum_{j\in\mathcal{E}} n_{\langle j\rangle} = \sum_{j\in\mathcal{E}} \epsilon_j n_{\langle \mathrm{r}\rangle}, \tag{C6}$$

the objective function can also be expressed by

$$F_j = n_j + \sum_{\substack{i\in\mathcal{S}\setminus\mathcal{E} \\ \hat{\epsilon}_i=\hat{\epsilon}_j}} \nu_{ij} n_i + \tilde{n}_{j,\min} - \epsilon_j n_{\langle \mathrm{r}\rangle}, \tag{C7}$$

which is the objective function used in FastChem 1. However, in contrast to FastChem 1, here, depending on the initial values of $n_{j,\min}^{(0)}$ and $n_0^{(0)}$, $n_{\langle \mathrm{r}\rangle}$ is not necessarily constant over the iteration procedure. That is why in FastChem 2 no additional iteration procedure is required to determine the fitting $n_{\langle \mathrm{r}\rangle}$.

This paper has been typeset from a TEX/LATEX file prepared by the author.

Downloaded from https://academic.oup.com/mnras/article/517/3/4070/6702739 by Universitaetsbibliothek Bern user on 08 March 2023